Research Square

Preprints are preliminary reports that have not undergone peer review.
They should not be considered conclusive, used to inform clinical practice,
or referenced by the media as validated information.

Divergent Actual Evapotranspiration Trends Across Global Biomes at Multiple Temporal Scales

mohamad kamangar
International Institute for Applied Systems Analysis
Sylvia Tramberend
International Institute for Applied Systems Analysis
Emilio Politti
International Institute for Applied Systems Analysis
Masoud Minaei
m.minaei@um.ac.ir

International Institute for Applied Systems Analysis

Research Article

Keywords: Actual Evapotranspiration, Terrestrial Biomes, Climate Change, Hydroclimatic Patterns, Spatial Variability

Posted Date: November 2nd, 2026

DOI: https://doi.org/10.21203/rs.3.rs-11296843/v1

License: This work is licensed under a Creative Commons Attribution 4.0 International License.
Read Full License

Additional Declarations: No competing interests reported.

Divergent Actual Evapotranspiration Trends Across Global Biomes at Multiple Temporal Scales

[1,2,3]Water Security Research Group, Biodiversity and Natural Resources Program, International Institute for Applied Systems Analysis (IIASA), Schlossplatz 1, A-2361 Laxenburg, Austria
[1,4]Department of Geography, Faculty of Letters and Humanities, Ferdowsi University of Mashhad, Mashhad, Iran
[4]Faculty of Humanities and Social Sciences, Department of Geography, University of Sakarya, Sakarya, Türkiye.
[4]Geographic Information Science/System and Remote Sensing Laboratory (GISSRS: Lab), Ferdowsi University of Mashhad, Mashhad, Iran

ABSTRACT

Global warming is not uniformly intensifying evapotranspiration across terrestrial Biomes rather, it is amplifying divergence between energy-limited and water-limited biomes. Analyzing 44 years (1980–2023) of GLEAM v4 ET estimates across 15 major terrestrial biomes, we show that most biomes (13 of 15) exhibit statistically significant positive ET trends ($p < 0.05$), with humid forest biomes and tundra accelerating water loss at rates of +0.8 to +1.46 mm yr^{-1}. In contrast, temperate grasslands and deserts exhibit declining ET (up to −0.15 mm yr^{-1}), suggesting water supply constraints despite warming. This divergence peaks during Northern Hemisphere spring and summer, when temperate forests show accelerating ET trends of +2.5 mm $decade^{-1}$ during May–August—equivalent to ~15% of their baseline warm-season ET. Critically, ET responses vary even within water-limited biomes: tropical grasslands show moderate increases (+0.28 mm yr^{-1}), contrasting sharply with declines in temperate grasslands and deserts, indicating divergent water availability controls. Unlike previous global-scale studies that aggregate across climate zones, our biome-resolved, multi-decadal analysis reveals that anthropogenic warming is driving divergent ET responses across terrestrial biomes, intensifying water loss in humid Biomes while exacerbating water scarcity in already-stressed drylands. These findings challenge assumptions of uniform hydrological intensification and provide observational constraints for Earth system models and adaptive water management strategies.

Keywords: Actual Evapotranspiration , Terrestrial Biomes, Climate Change, Hydroclimatic Patterns , Spatial Variability.

Introduction

Evapotranspiration is a key land–atmosphere flux that integrates hydrological, energetic, and biophysical processes, while also reflecting the strong coupling between terrestrial water loss and carbon uptake (Gentine et al., 2019; Liu et al., 2021). Long-term ecosystem-scale flux observations from the global eddy covariance network have revealed how evapotranspiration and carbon fluxes co-vary across timescales and environmental gradients, offering critical insights into emerging trends and feedbacks between terrestrial ecosystems and climate change (Xiao et al., 2026). Its significance is particularly acute in water-limited environments, where ET can account for over 90% of annual precipitation (Flerchinger et al., 1996; Maruyama et al., 2025), and its tight coupling with stomatal conductance, canopy structure, and soil moisture availability makes it a sensitive indicator of land-surface functioning under global change (Helbig et al., 2020; Giardina, 2023). Under anthropogenic warming, however, actual evapotranspiration (ET_a) responses diverge fundamentally across ecosystems: energy-limited biomes—typically cold and humid—experience amplified ET_a through extended growing seasons and vegetation greening (Helbig et al., 2020; Hofmann et al., 2025), while water-limited drylands face intensified atmospheric demand that is increasingly decoupled from actual water flux due to soil moisture depletion and physiological stress (Berg et al., 2016; Alsafadi et al., 2024). This biome-contingent divergence implies that global warming does not uniformly intensify the terrestrial water cycle but instead exacerbates pre-existing hydroclimatic disparities—a pattern with profound implications for carbon cycling, ecosystem resilience, and water resource management (Pan et al., 2019).

Recent studies have documented positive ET_a trends globally, yet critical gaps remain in understanding biome-specific responses and their seasonal dynamics. Pan et al. (2020) reported increasing ET_a across the continental U.S., while Zhu et al. (2016) identified significant increases in temperate forests and croplands but stagnation or decline in boreal regions, and Martens et al. (2017) linked positive ET trends over Europe to rising leaf area index. However, these studies

share three structural limitations: reliance on annual or seasonal aggregation that obscures intra-annual hydroclimatic dynamics; temporal spans insufficient to capture multi-decadal trend stabilization; and spatial resolutions or domain boundaries that preclude globally coherent, biome-specific attribution. Critically, the degree to which ETa trends diverge across the full spectrum of terrestrial biomes—and the seasonal timing of that divergence—remains unresolved. This gap directly impairs the capacity of Earth system models to accurately partition surface energy and water fluxes across heterogeneous land surfaces and limits the ability of water resource managers to anticipate biome-specific vulnerabilities under accelerating climate change. We address this gap by presenting a comprehensive, biome-explicit analysis of ET_a trends across 15 principal terrestrial biomes over a 44-year period (1980–2023), leveraging the high-resolution GLEAM v4 dataset. Specifically, we ask: (i) How do long-term ETa trends diverge across terrestrial biomes, and what hydroclimatic mechanisms drive this divergence? (ii) What is the intra-annual structure of ETa change, and during which seasons does warming most strongly amplify or suppress evapotranspiration? (iii) To what extent does global warming exacerbate pre-existing hydroclimatic disparities rather than producing uniform intensification of the terrestrial water cycle? Unlike previous global-scale studies that aggregate across climate zones or focus on regional domains, our biome-resolved, multi-decadal analysis integrates annual and sub-annual perspectives within a unified analytical framework, providing mechanistic insights into land-surface responses to climate change. The remainder of this paper is organized as follows: Section 2 describes the data and methods; Section 3 presents biome-specific ET_a trends at annual and seasonal scales; Section 4 discusses the hydroclimatic mechanisms driving divergent responses and their implications for Earth system modeling and water resource management; and Section 5 summarizes the key findings and future research directions.

Data and Methodology

Study Area

The study area includes the entire terrestrial surface of the Earth, classified into 15 major terrestrial biomes and 846 Ecoregions, based on an ecoregion-based approach for housing conservation (Dinerstein et al., 2017; https://ecoregions.appspot.com). This classification provides a biographical framework that integrates ecological, climate and biological characteristics, which enables spatial analysis of ET_a in separate ecological regions (Fig 1). Biome includes a wide range of Biomes, from dry desert and temperate forests to tropical rainfall and boreal Biome, performing each unique climate and vegetative patterns that affect ET_a dynamics.

Ecoregion boundaries are particularly relevant to analyze spatial variability in ET_a, as they depict areas of ecological transitions that are sensitive to environmental changes.

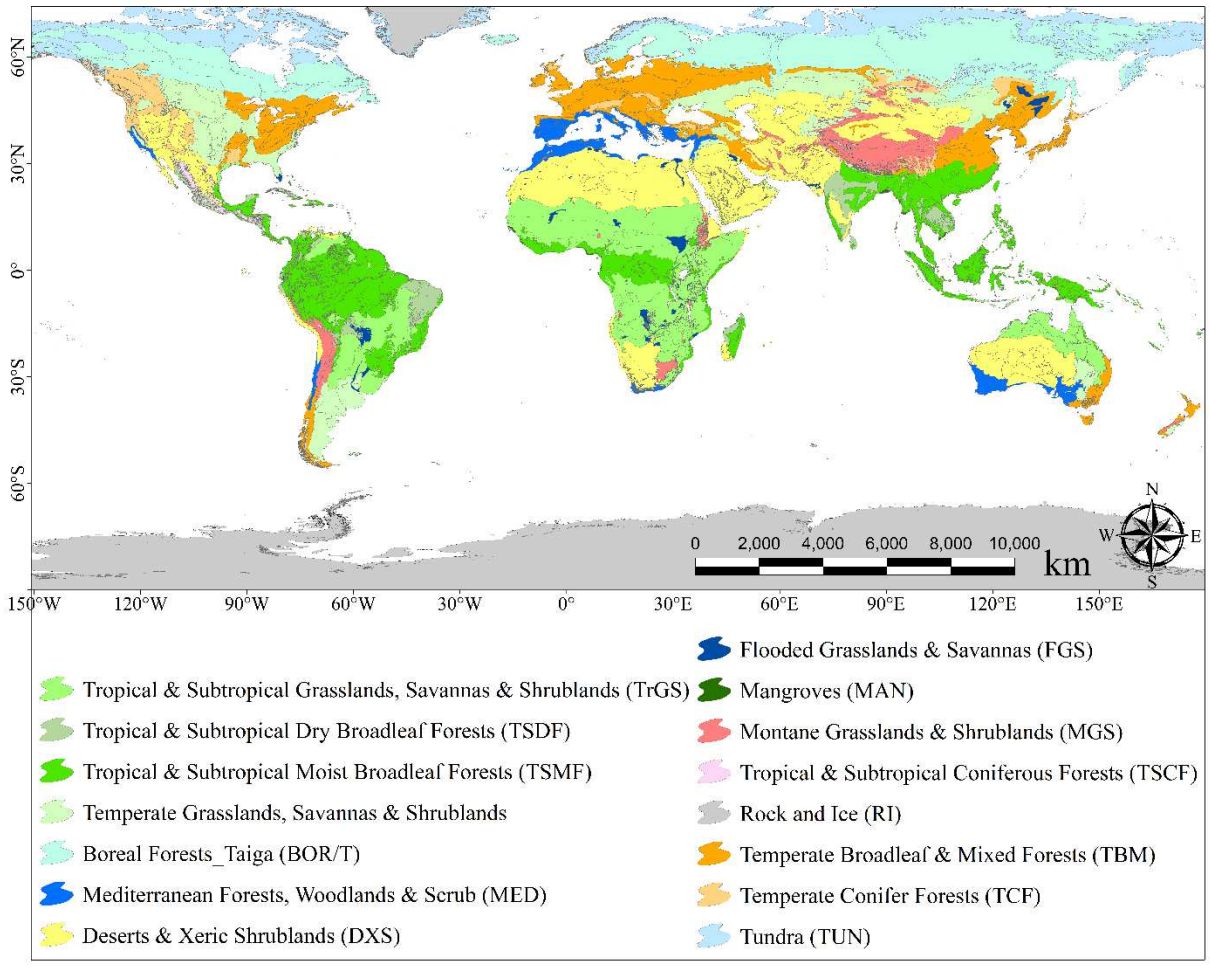


Fig 1. Global spatial distribution of terrestrial biomes analyzed in this study, highlighting the diversity of land cover types across the Earth's surface.

Datasets

We utilized the most recent release of the Global Land Evaporation Amsterdam Model (GLEAM v4), which delivers annual terrestrial ET_a estimates from 1980 to 2023 at 0.1° spatial resolution across the global land surface. Annual data were deliberately selected to suppress short-term variability and seasonal noise, thereby enabling clearer identification of long-term trends in water fluxes at the global pixel scale. GLEAM v4 combines advanced hybrid modeling techniques with extensive eddy-covariance and sap-flow observations to substantially enhance the accuracy of both evapotranspiration and evaporative-stress estimates. The dataset provides ET_a along with its core components (transpiration, soil evaporation, and interception loss), as well as root-zone soil

moisture, potential evaporation, sensible heat flux, and evaporative stress. GLEAM v4 demonstrates strong skill in capturing atmospheric demand, soil-moisture controls, and plant water use, with high agreement against global flux-tower observations (median r = 0.73–0.95; KGE = 0.49; RMSE = 0.95 mm d^{-1}; Miralles et al., 2016), performing comparably or better than MOD16 and LSA-SAF (Guo et al., 2022; Martens et al., 2017) and ranking alongside PT-JPL as a top global product in WACMOS-ET assessments, with version-4 improvements reducing evaporative-stress errors by 15–20% (Miralles et al., 2025).

Methods

The Modified Mann-Kendall

To detect long-term trends in annual ET_a, we applied the Modified Mann-Kendall (MMK) test (Hamed & Rao, 1998), which accounts for temporal autocorrelation in climate time series. The Mann-Kendall test is a widely used non-parametric method that does not require assumptions of normality, making it suitable for pixel-based geophysical datasets (Kendall, 1975; Mann, 1945). However, positive autocorrelation—common in climate variables such as ET_a can inflate Type I error rates and lead to spurious trend detection (von Storch, 1995). The MMK test addresses this issue by correcting the variance of the test statistic based on the autocorrelation structure of the data. Trend Magnitude Estimation The magnitude of the trend was estimated using Sen's slope estimator (Sen, 1968), a robust non-parametric method calculated as the median of all pairwise slopes was calculated using Equation 1:

$$\hat{Q} = \text{median}\left[\frac{(x_j - x_k)}{j-k}\right] \quad \text{for all } j > k \qquad (1)$$

where x_j and x_k are data values at times j and k, respectively, and $\hat{Q}$ represents the rate of change over time Autocorrelation Correction For each pixel, the lag-1 autocorrelation coefficient (r_1) was computed Equation 2:

$$r_1 = \frac{\sum_{t=1}^{n-1}(x_t - \bar{x})(x_{t+1} - \bar{x})}{\sum_{t=1}^{n}(x_t - \bar{x})^2} \qquad (2)$$

where n = 44 years (1980–2023) and $\bar{x}$ is the mean of the time series. The variance of the Mann-Kendall statistic S was then corrected following Hamed & Rao (1998) using Equation 3:

$$V^*(S) = V(S) \times \left[1 + \frac{2}{n(n-1)(n-2)} \sum_{i=1}^{n-1}(n-i)(n-i-1)(n-i-2)\rho_i\right] \quad (3)$$

where $V(S) = n(n-1)(2n+5)/18$ is the uncorrected variance, and ρ_i is the autocorrelation at lag i (computed up to lag 10 following Hamed & Rao, 1998). Mann-Kendall Statistic The Mann-Kendall statistic S was calculated Equation 4:

$$S = \sum_{k=1}^{n-1} \sum_{j=k+1}^{n} sgn(x_j - x_k) \quad (4)$$

where the sign function was calculated equation 5:

$$sgn(x_j - x_k) = \begin{cases} +1 & if \quad (x_j - x_k) > 0 \\ 0 & if \quad (x_j - x_k) = 0 \\ -1 & if \quad (x_j - x_k) < 0 \end{cases} \quad (5)$$

The standardized test statistic Z was calculated equation 6:

$$Z = \begin{cases} x = \dfrac{S-1}{\sqrt{\text{var}(s)}} & \begin{cases} if & S > 0 \\ if & S = 0 \\ if & S < 0 \end{cases} \\ x = \dfrac{S+1}{\sqrt{\text{var}(s)}} \end{cases} \quad (6)$$

Multiple Testing Correction Given the large number of spatial pixels tested (n = 2132298 pixels), we controlled for multiple comparisons using the False Discovery Rate (FDR) procedure (Benjamini & Hochberg, 1995) at q = 0.05. The FDR method controls the expected proportion of false positives among all rejected null hypotheses, making it more powerful than the Bonferroni correction for large-scale spatial analyses (Wilks, 2016). Only pixels with FDR-adjusted p-values < 0.05 were classified as exhibiting significant trends. The mean lag-1 autocorrelation across all pixels was $r_1 = 0.42 \pm 0.18$ (mean ± SD), justifying the use of the MMK test over the standard Mann-Kendall test. All analyses were performed in R version 4.3.2 (R Core Team, 2023) using the modifiedmk package version 1.6.0 (Patakamuri & O'Brien, 2020) with parallel processing across 8 CPU cores.

Results

Median ET_a was computed for all pixels belonging to each biome, and the resulting values are reported to document the central ET_a conditions across the full biome set. The analysis shows that the highest median ET_a occurs in tropical and subtropical moist broadleaf forests (1181.41 mm yr^{-1}), while the lowest value is observed in rock and ice surfaces (23.85 mm yr^{-1}); the full pattern and detailed values are presented in Fig 1. These values represent the median ET_a associated with each biome, derived from the full set of contributing pixels without additional transformations or grouping. The biomes are reported individually, and each median corresponds directly to the spatially aggregated ETa records assigned to that biome category. Figure 2 provides the visual representation of these biome-level medians, with one bar displayed for each biome to reflect the calculated central ET_a value.

The median ET_a values across all biomes spanned a numerical range from 23.85 to 1181.41 mm yr^{-1}, corresponding to the minimum (Rock & Ice) and maximum (Tropical & Subtropical Moist Broadleaf Forests) reported medians. The difference between these two values is 1157.56 mm yr^{-1}. Considering the distribution of biomes across numerical intervals, six biomes had median ET_a values above 600 mm yr^{-1}, while six biomes fell between 300- and 600-mm yr^{-1}. Additionally, three biomes exhibited median ET_a values below 200 mm yr^{-1}.

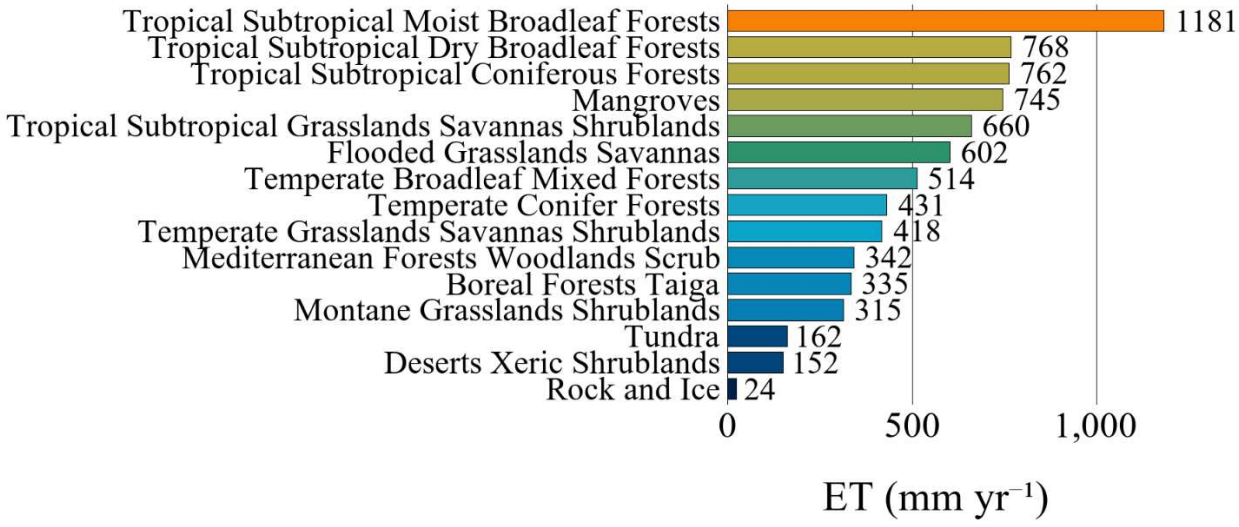


Fig 2. Median Annual ET_a 1980-2023

Long-term trends in annual ET_a were analyzed across 15 terrestrial biomes worldwide (Figure 3). All reported trends are statistically significant at the 95% confidence level ($p < 0.05$). The computed trends ranged from +1.46 mm/year in Temperate Broadleaf and Mixed Forests to −0.15 mm/year in Temperate Grasslands, Savannas, and Shrublands.

Thirteen of the 15 biomes exhibited positive ET_a trends, while two showed negative trends. The strongest increases were observed in Temperate Broadleaf and Mixed Forests (+1.46 mm/year), Montane Grasslands and Shrublands (+0.83 mm/year), and Boreal Forests (+0.82 mm/year). Moderate positive trends were found in Tropical and Subtropical Moist Broadleaf Forests (+0.66 mm/year), Mangroves (+0.66 mm/year), and Tropical and Subtropical Coniferous Forests (+0.59 mm/year). Tundra exhibited an increase of +0.54 mm/year, while Tropical and Subtropical Dry Broadleaf Forests and Temperate Conifer Forests displayed trends of +0.50 and +0.46 mm/year, respectively. Lower positive trends were observed in Flooded Grasslands and Savannas (+0.35 mm/year) and Tropical and Subtropical Grasslands, Savannas, and Shrublands (+0.28 mm/year). Minimal changes occurred in Rock and Ice-dominated areas (+0.04 mm/year) and Mediterranean Forests, Woodlands, and Scrub (+0.03 mm/year). Negative trends were detected in Deserts and Xeric Shrublands (−0.08 mm/year) and Temperate Grasslands, Savannas, and Shrublands (−0.15 mm/year). Overall, the majority of terrestrial biomes experienced increasing ET_a over the study period, with only two biomes showing decline.

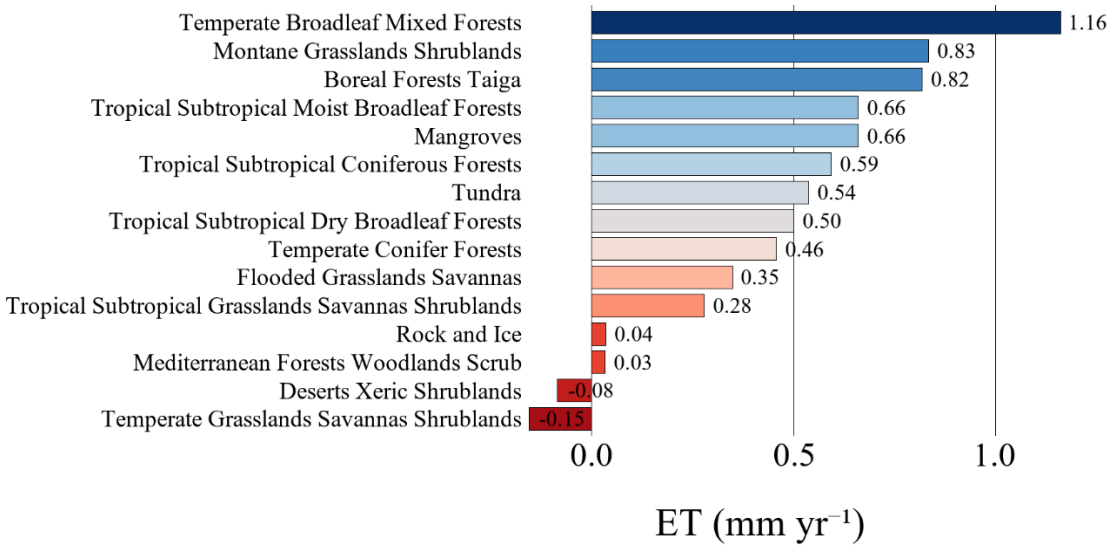


Fig 3. Biome-Level Averages of Long-Term ET_a Trends (mm/year)

Seasonal Analysis

Seasonal trends vary substantially across biomes. Winter displays the most heterogeneous pattern among seasons. Increasing trends dominate in most biomes, led by Temperate Broadleaf & Mixed Forests (92.73%), Rock & Ice (88.23%), and Temperate Conifer Forests (81.21%). Montane Grasslands & Shrublands (76.51%), Temperate Grasslands, Savannas & Shrublands (76.66%), Tropical & Subtropical Coniferous Forests (67.17%), Tropical & Subtropical Moist Broadleaf Forests (63.90%), Mangroves (64.24%), Flooded Grasslands & Savannas (60.13%), Tropical & Subtropical Dry Broadleaf Forests (72.28%), Tundra (66.75%), and Deserts & Xeric Shrublands (48.22%) also show notable proportions of increasing pixels. Boreal Forests/Taiga2 is the only winter biome where decreasing pixels are predominant (58.85% decreasing vs. 41.15% increasing). Non-significant pixels remain very low across all biomes, typically below 5%.

Spring is characterized by widespread increasing trends across nearly all biomes. Boreal Forests/Taiga2 exhibits the highest proportion of increasing pixels (96.54%), followed by Temperate Broadleaf & Mixed Forests (92.72%) and Tundra (90.96%). Temperate Conifer Forests (82.44%), Montane Grasslands & Shrublands (78.24%), Flooded Grasslands & Savannas (66.58%), Tropical & Subtropical Moist Broadleaf Forests (65.29%), Tropical & Subtropical Dry Broadleaf Forests (69.83%), Tropical & Subtropical Coniferous Forests (58.27%), Tropical & Subtropical Grasslands, Savannas & Shrublands (58.24%), Mangroves (58.43%), Mediterranean Forests, Woodlands & Scrub (58.49%), Temperate Grasslands, Savannas &

Shrublands (69.53%), and Rock & Ice (69.41%) also display dominant increasing trends. The only exception is Deserts & Xeric Shrublands, where decreasing pixels prevail (56.09% decreasing vs. 39.05% increasing). Non-significant pixels remain minimal, typically under 5%.

Summer maintains widespread increasing trends, with the highest proportions in Temperate Broadleaf & Mixed Forests and Boreal Forests/Taiga2 (92.09% each), followed by Tundra (85.15%), Montane Grasslands & Shrublands (76.85%), Tropical & Subtropical Moist Broadleaf Forests (68.27%), Mangroves (67.84%), Flooded Grasslands & Savannas (67.00%), Tropical & Subtropical Coniferous Forests (72.08%), Temperate Conifer Forests (71.22%), Tropical & Subtropical Dry Broadleaf Forests (59.51%), Temperate Grasslands, Savannas & Shrublands (55.33%), Tropical & Subtropical Grasslands, Savannas & Shrublands (55.88%), Rock & Ice (36.76%), and Mediterranean Forests, Woodlands & Scrub (41.30%). Decreasing pixels dominate in Deserts & Xeric Shrublands (62.46%), Rock & Ice (63.22%), and Mediterranean Forests, Woodlands & Scrub (57.80%), while non-significant pixels remain below 2% in most biomes.

Autumn again shows predominantly increasing trends. Rock & Ice exhibits the highest proportion of increasing pixels (93.95%), followed by Temperate Broadleaf & Mixed Forests (87.15%), Boreal Forests/Taiga (84.15%), Mangroves (71.41%), Tropical & Subtropical Moist Broadleaf Forests (71.53%), Tropical & Subtropical Coniferous Forests (77.49%), Montane Grasslands & Shrublands (78.72%), Flooded Grasslands & Savannas (64.20%), Tropical & Subtropical Grasslands, Savannas & Shrublands (61.13%), and Tropical & Subtropical Dry Broadleaf Forests (66.70%). Decreasing pixels are mainly observed in Deserts & Xeric Shrublands (52.71%) and Mediterranean Forests, Woodlands & Scrub (50.76%). Non-significant pixels remain below 2% across all biomes.

Overall, across all seasons and biomes, increasing ET_a trends are spatially widespread, with 49 of 56 biome–season combinations (87.5%) showing more than 50% of pixels with significant increases. Only seven combinations (12.5%) exhibit a majority of decreasing pixels: Deserts & Xeric Shrublands (spring, summer, autumn), Mediterranean Forests, Woodlands & Scrub (summer, autumn), Rock & Ice (summer), and Boreal Forests/Taiga (winter). Non-significant trends account for a small fraction of pixels (<10%), and typically remain below 1% in most biome–season pairs (fig. 4).

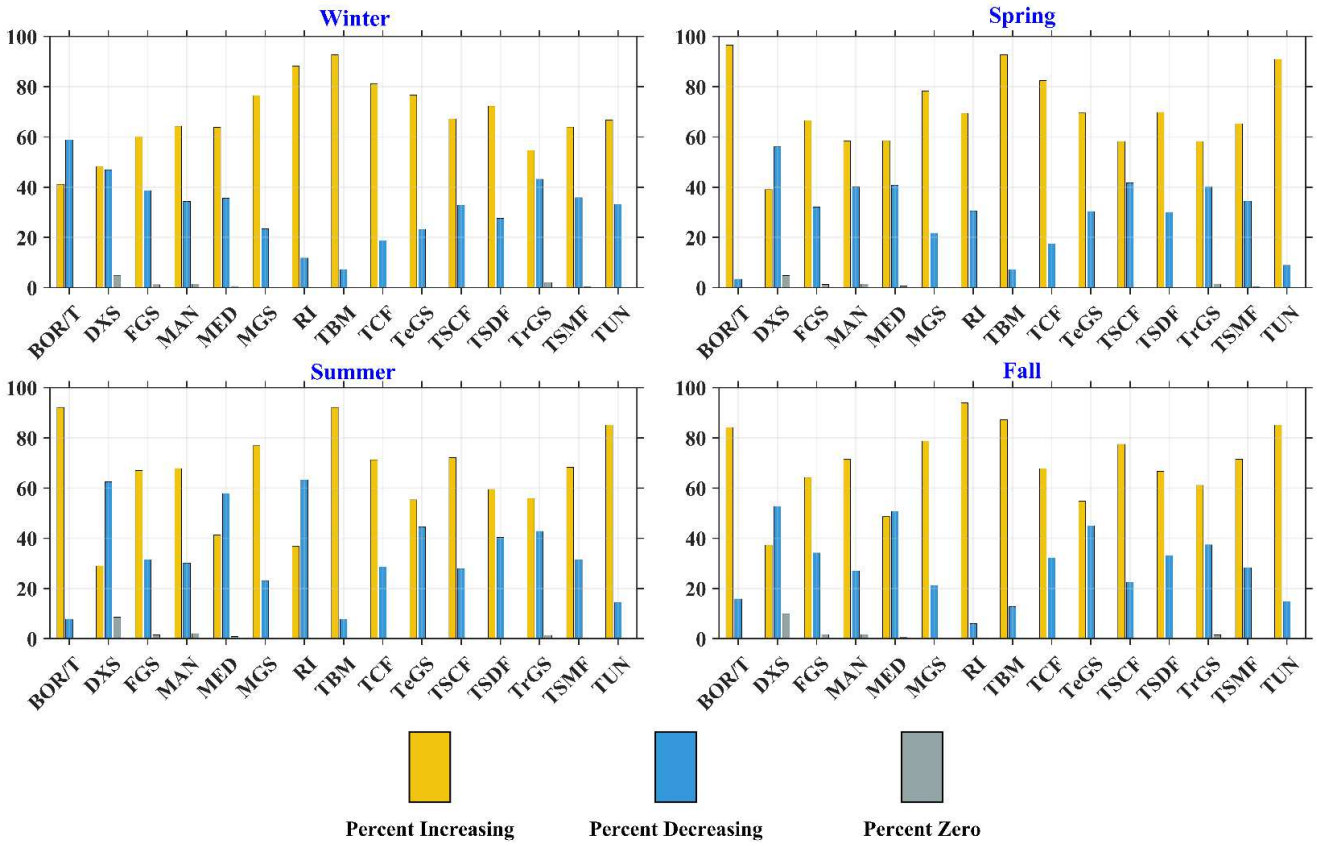


Fig 4. Seasonal ET_a trends across biomes: % of pixels with significant increases, declines, or nonsignificant changes

Seasonal ET_a trends displayed clear biome-dependent behavior. Winter showed the weakest signals, with most slopes clustering near zero; even in biomes with positive responses, magnitudes generally remained below ~0.10. In spring, ET_a increased across the majority of biomes, with several forested systems exhibiting moderate slopes on the order of 0.3–0.5, reflecting the rapid transition in energy and moisture availability.

Summer presented the strongest and most spatially extensive intensification, particularly in temperate and boreal forests where slopes frequently exceeded 0.5 (e.g., approximately 0.76 in Temperate Broadleaf & Mixed Forests), indicating robust seasonal amplification of ET_a. In contrast, arid and semi-arid biomes consistently showed weak or negative responses across seasons, with summer declines on the order of −0.08 to −0.10 in water-limited regions. Autumn trends were generally moderate, combining positive responses in several mesic biomes with noticeable negative slopes in Mediterranean and temperate grassland systems. Overall, 75% of biome–season combinations exhibited positive Sen slopes, while meaningful negative trends were

largely restricted to arid and seasonally water-limited Biomes. The complete distribution of seasonal trend magnitudes across all 15 biomes is synthesized in the heatmap (Figure 6).

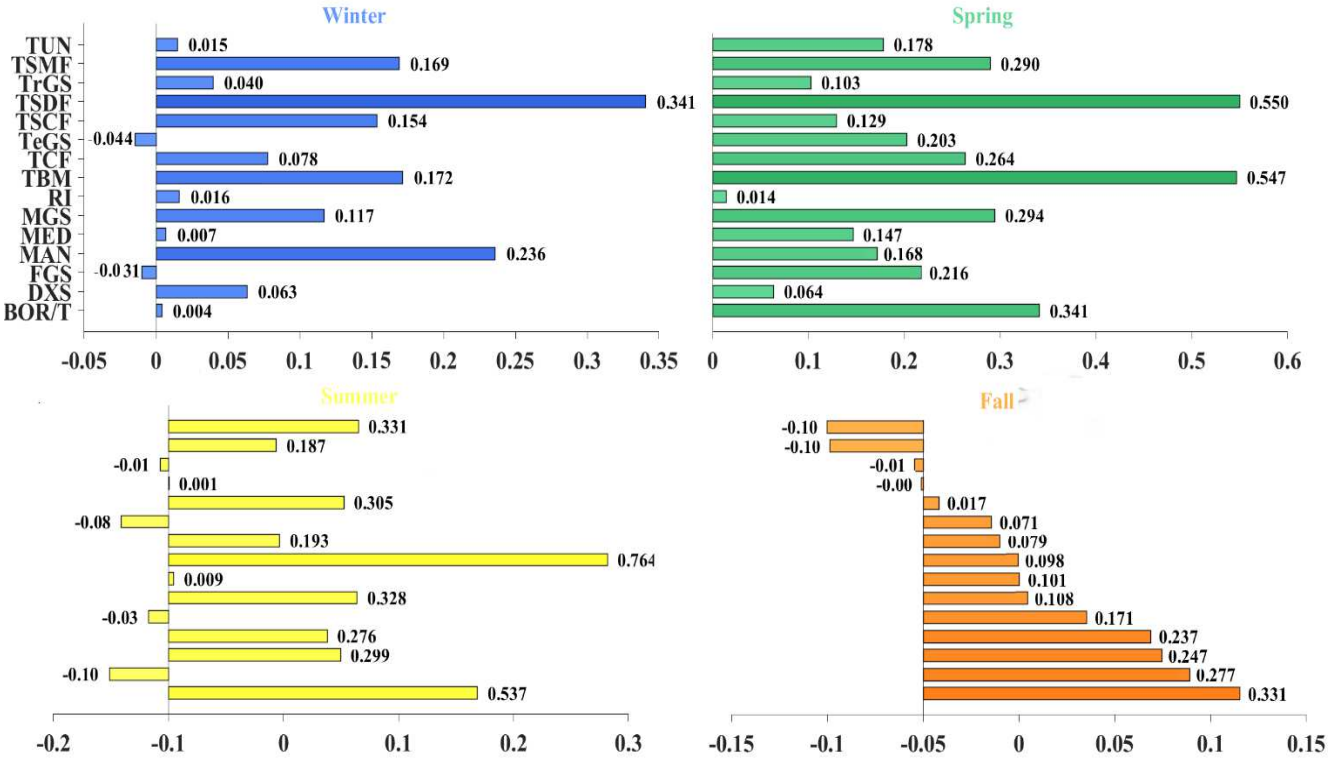


Fig 5. Seasonal ET_a trends within each biome, showing the proportion of pixels with significant increases, declines, or nonsignificant changes ($p \geq 0.05$).

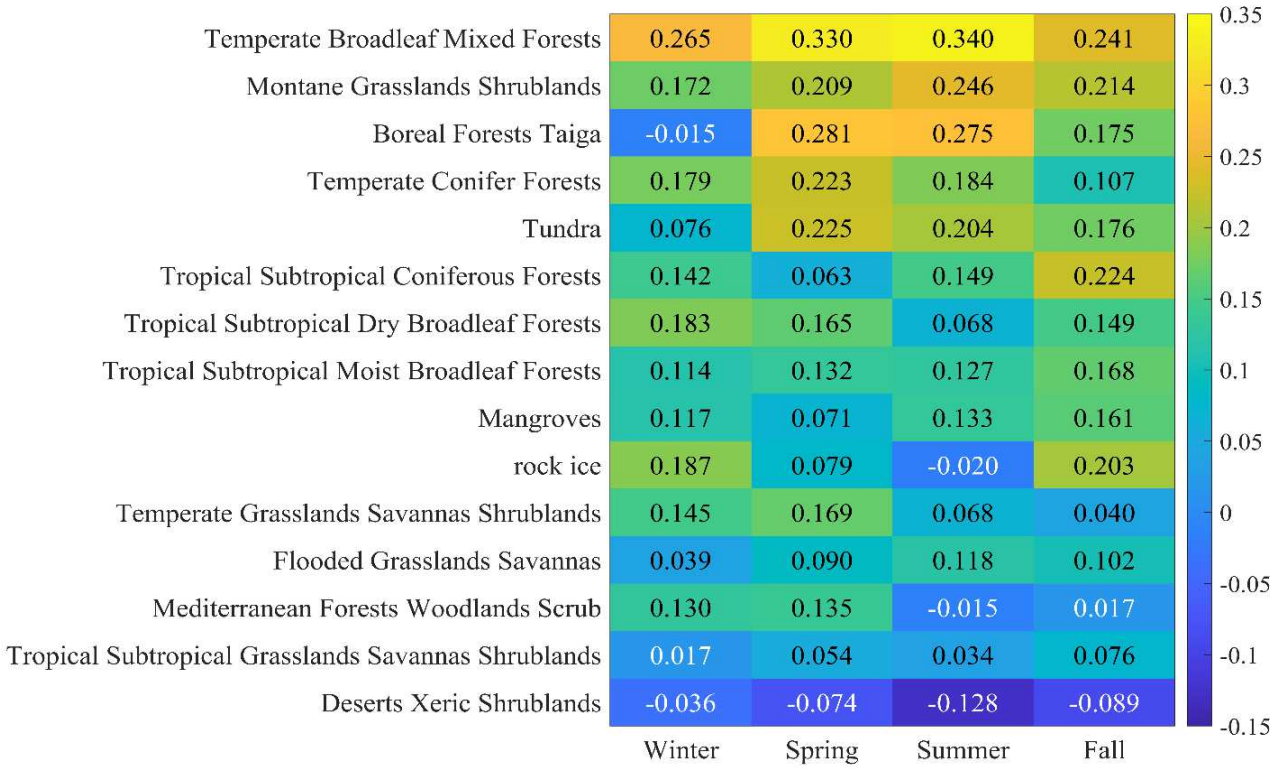


Fig 6. Seasonal heatmap of mean Tau (τ) for each biome. Blue represents lower values, red higher values, and light gray indicates intermediate or near-zero values.

Monthly Analysis

Monthly ET_a trends exhibited distinct seasonal patterns across biomes (Figure 7). Of the 168 biome–month combinations analyzed, 141 (83.9%) showed a majority of pixels with increasing ET_a, while only 27 (16.1%) exhibited predominantly decreasing trends. Non-significant trends were rare, with fractions below 18% for all biomes and months, and mostly under 5%. During the Northern Hemisphere growing season (March–September), Boreal Forests/Taiga, Temperate Broadleaf and Mixed Forests, and Tundra consistently exhibited the highest fractions of increasing pixels (typically >85%). Conversely, Deserts and Xeric Shrublands, along with Mediterranean Forests, showed persistent decreasing trends during summer months (June–August), with decreasing pixel fractions exceeding 50%. An unexpected pattern emerged in Boreal Forests/Taiga during winter months (November–February), where the biome shifted from predominantly increasing trends in other seasons to majority decreasing trends (>54% decreasing pixels). Rock and Ice-dominated areas displayed contrasting seasonal behavior, with majority decreases in spring (March–April) but strong increases in autumn and early winter (September–December).



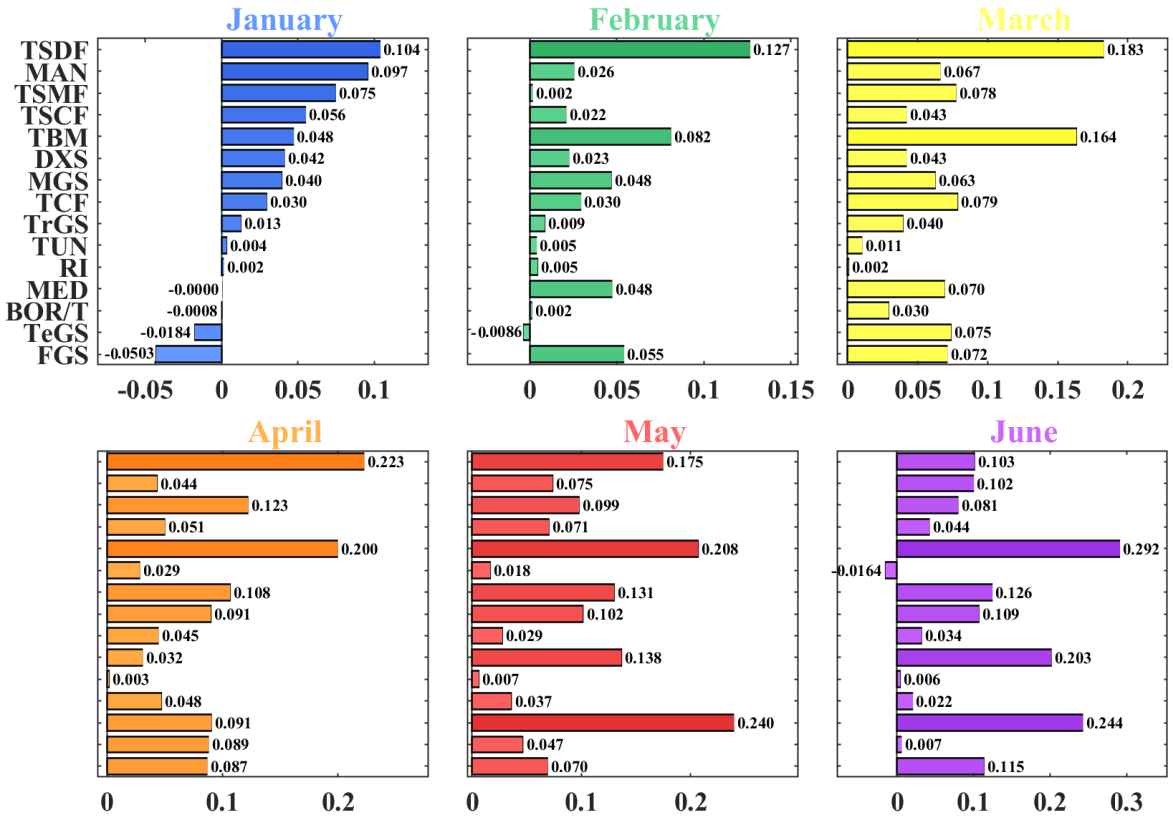
Fig 7. Monthly ETa changes across global biomes. Of 168 biome–month combinations, 141 (83.9%) showed >50% increasing pixels, while 27 (16.1%) had >50% decreasing pixels; non-significant changes were <18%.

Sen's slope analysis (Figure 8) revealed that monthly ET_a trends ranged from +0.292 mm/month (Temperate Broadleaf and Mixed Forests in June) to -0.164 mm/month (Deserts and Xeric Shrublands in June). The strongest positive trends occurred during the Northern Hemisphere warm season (April–August), with peak values in June–July. Temperate Broadleaf and Mixed Forests exhibited the highest monthly increases in May (0.208 mm/month) and June (0.292 mm/month), followed by Boreal Forests/Taiga (peaking at 0.244 mm/month in June) and Tundra (0.203 mm/month in July). Tropical and Subtropical Dry Broadleaf Forests showed a distinct seasonal pattern, with strong increases during the dry season (January–April, peaking at 0.223 mm/month in April) but a notable decline in July (-0.061 mm/month).

Negative trends were concentrated in water-limited biomes and temperate grasslands, particularly during summer and autumn months. Deserts and Xeric Shrublands exhibited the strongest negative trend in June (-0.164 mm/month). Mediterranean Forests showed notable declines during their dry season, with the greatest decrease in October (-0.073 mm/month). Across all 168 biome–month combinations, 145 (86.3%) exhibited positive slopes, while 23 (13.7%) displayed negative slopes, with negative trends largely confined to arid, Mediterranean, temperate grassland, and tropical dry forest biomes during their respective dry or dormant seasons.

Kendall's tau values ranged from +0.29 (Temperate Broadleaf and Mixed Forests in June) to -0.22 (Deserts and Xeric Shrublands in June) (Figure 9), indicating weak to moderate but statistically significant trends across global biomes. The spatial and temporal distribution of these correlations revealed distinct seasonal patterns closely aligned with regional phenological cycles. The strongest positive correlations emerged during the Northern Hemisphere warm season (April–August), when vegetation activity peaks and water availability is generally sufficient to support enhanced evapotranspiration. June represented the critical inflection point, with Temperate Broadleaf and Mixed Forests exhibiting the highest correlation (τ =0.29), followed closely by Boreal Forests/Taiga (τ = 0.27) and Tundra (τ = 0.24). These biomes, characterized by pronounced seasonal growth cycles, demonstrated robust upward trends in ET_a during their peak growing season, reflecting intensified vegetation productivity and atmospheric water demand under changing climatic conditions. In contrast, negative correlations appeared primarily in water-limited biomes during their respective dry seasons, highlighting the vulnerability of these Biomes to moisture stress. Deserts and Xeric Shrublands showed the strongest negative trend (τ = -0.22 in June), coinciding with peak aridity and minimal vegetation cover. Mediterranean

Forests exhibited their most pronounced decline in October (τ = -0.18), during the characteristic Mediterranean dry summer-autumn transition, while Tropical and Subtropical Dry Broadleaf Forests displayed moderate negative trends in July (τ = -0.10), corresponding to the dry season in many tropical regions. Despite these localized declines, the overall pattern was dominated by positive trends, with 86.3% of biome-month combinations exhibiting upward ET_a trajectories, underscoring a widespread intensification of the terrestrial water cycle across diverse Biomes.



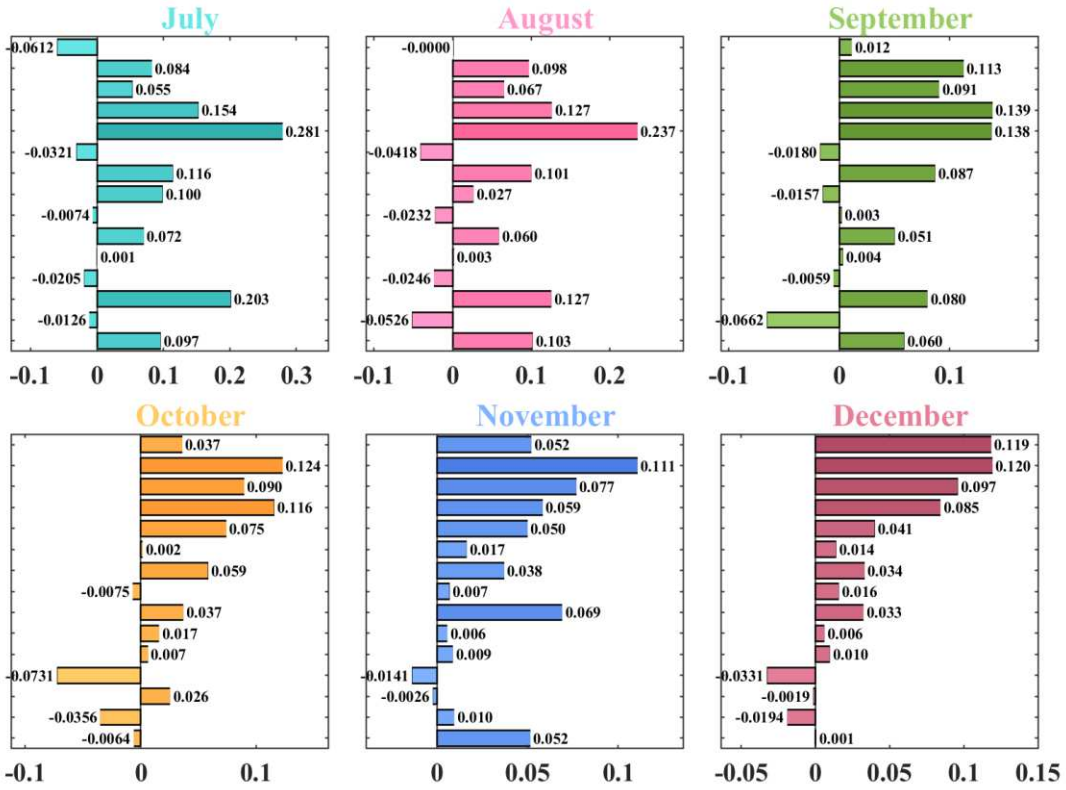


Fig 8. Monthly Sen's slope values across biomes (mm month^{-1})

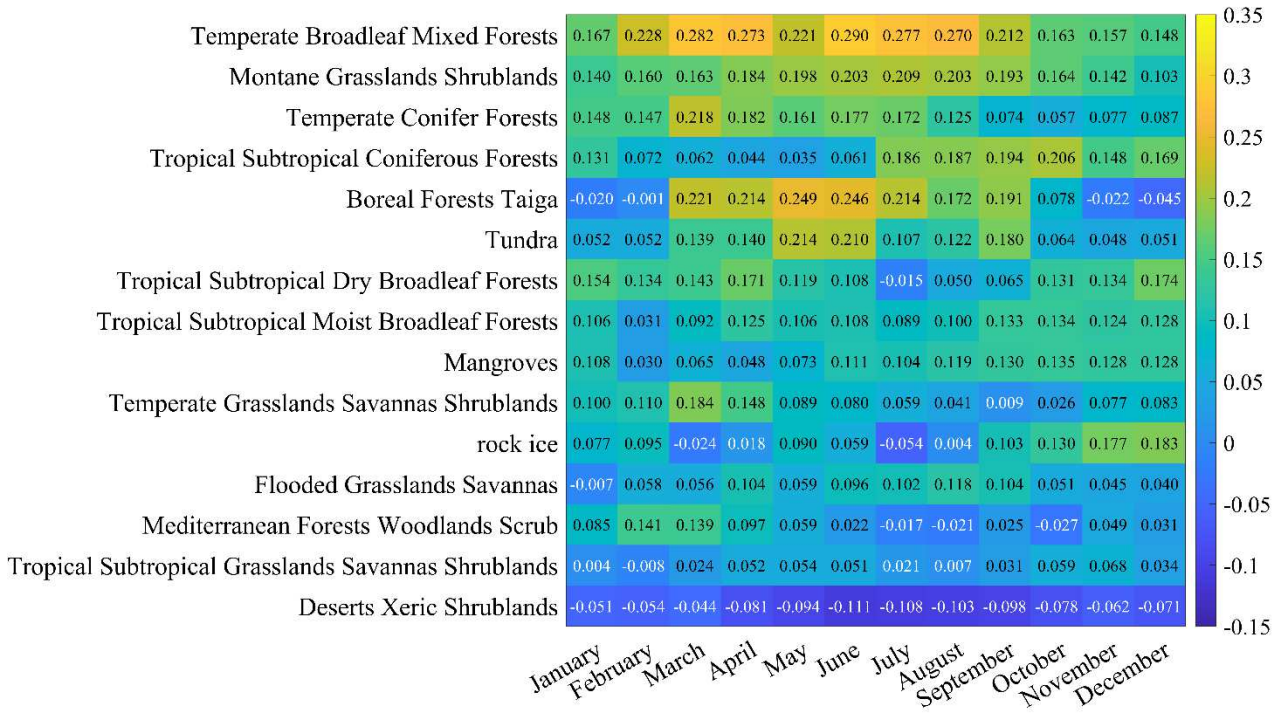


Fig 9. Heatmap showing the monthly mean Tau (τ) for each biome.

Discussion

Across the global terrestrial biosphere, ET_a is increasingly emerging not as a stationary hydrological flux, but as a dynamically reorganizing component of the Earth system that reflects the combined effects of climatic warming, vegetation change, atmospheric evaporative demand, and ecosystem water limitation. The predominance of positive ET_a trends across most global biomes in this study, particularly within temperate and boreal forest systems, provides strong evidence for an ongoing intensification of the terrestrial water cycle under contemporary climate change. This large-scale behavior is consistent with recent global assessments reporting accelerating ET increases since the 1980s driven by vegetation greening, rising vapor pressure deficit, and enhanced atmospheric energy availability (Zhang et al., 2015; Yang et al., 2023). However, the present findings further demonstrate that this intensification is highly biome-dependent and seasonally asymmetric rather than spatially uniform. Forested and energy-limited Biomes exhibited the strongest positive responses, whereas arid and seasonally water-limited biomes frequently displayed weak or negative trends, especially during warm-season months. Such divergence suggests that the global ET response is increasingly governed by the interaction between atmospheric demand and hydrological constraints, reinforcing the emerging view that hydroclimatic responses to warming are strongly modulated by ecosystem-specific moisture accessibility and vegetation regulation mechanisms (Giardina et al., 2023; Hayat et al., 2025). In this context, the observed dominance of increasing ET_a trajectories across 86% of biome–month combinations indicates that large portions of the terrestrial biosphere are undergoing sustained hydroclimatic amplification, while simultaneously revealing the growing vulnerability of dryland Biomes where water availability can no longer compensate for rising evaporative demand.

The magnitude and spatial organization of ET_a trends identified in this study broadly agree with previous global and regional investigations, while also revealing important biome-scale distinctions that are often unresolved in coarse-scale analyses. The strong increases observed in temperate broadleaf and mixed forests, boreal forests, and tundra Biomes are highly consistent with the greening-induced ET amplification reported by Zhang et al. (2015) and the northern high-latitude intensification highlighted by Yang et al. (2023). Likewise, the predominance of positive ET_a trends in humid and energy-limited environments aligns with Li et al. (2021), who demonstrated that vapor pressure deficit and radiative forcing increasingly dominate ET dynamics in moisture-sufficient regions. Nevertheless, unlike many previous studies that focused primarily

on annual averages or continental-scale aggregation, the present biome-resolved analysis reveals pronounced seasonal contrasts, including winter declines in Boreal Forests/Taiga and persistent summer decreases across Deserts and Xeric Shrublands and Mediterranean systems. These patterns suggest that warming-driven ET enhancement is not universally sustained throughout the annual cycle and may weaken or reverse under severe moisture stress. Such findings are consistent with studies emphasizing hydrological limitations on ET responses under progressing drought conditions (Giardina et al., 2023) and with evidence that increasing atmospheric evaporative demand can exceed ecosystem water supply capacity in drylands (Albano et al., 2022). Furthermore, the observed negative summer responses in water-limited Biomes correspond closely with earlier sensitivity analyses showing that ET in arid climates is highly responsive to temperature, wind speed, and vapor pressure variability (Goyal, 2004; Tabari & Talaee, 2014). Compared with existing ET products and fusion datasets, the present analysis also benefits from the enhanced process representation and high-resolution structure of GLEAM4, which incorporates hybrid stress learning, groundwater accessibility, and improved soil moisture constraints (Miralles et al., 2024). This likely contributed to the clearer biome differentiation and stronger detection of seasonal heterogeneity relative to many previous large-scale ET assessments.

The strong seasonal and monthly asymmetries identified across global biomes also provide important mechanistic insight into the climatic controls governing ET_a variability under ongoing warming. The concentration of the strongest positive Sen slopes and Kendall's tau values during the Northern Hemisphere growing season, particularly in June and July, indicates that vegetation activity and atmospheric demand are becoming increasingly synchronized in energy-limited Biomes. The exceptionally strong positive responses observed in temperate broadleaf forests, boreal systems, and tundra biomes likely reflect the combined influence of vegetation greening, extended growing seasons, snow-cover decline, and warming-enhanced transpiration efficiency in high-latitude environments (Feng et al., 2018; Yang et al., 2023). In contrast, the persistent summer and autumn declines detected in Mediterranean and desert Biomes indicate a transition toward stronger hydrological limitation, where increasing vapor pressure deficit and declining soil moisture suppress evapotranspiration despite rising temperatures. Similar nonlinear ET responses to water deficit have been documented using flux-based and deep-learning approaches, which demonstrate that grasslands, shrublands, and dry Biomes experience abrupt ET reductions once critical moisture thresholds are exceeded (Giardina et al., 2023). The contrasting behavior

between humid and arid biomes observed here therefore supports the growing consensus that future ET trajectories will increasingly depend on the balance between energy availability and ecosystem water accessibility rather than temperature alone. Moreover, the observed seasonal redistribution of ET_a signals, particularly the enhanced cold-season increases across several high-latitude biomes, is consistent with broader evidence that climate warming is reorganizing hydrological seasonality and intensifying terrestrial moisture fluxes at multiple temporal scales (Ma et al., 2018; Allan et al., 2020). Collectively, these findings suggest that global ET_a dynamics are entering a phase of increasing hydroclimatic divergence, in which vegetation-rich and energy-limited systems continue to intensify, while dryland Biomes progressively approach hydrological thresholds that constrain evaporative resilience under continued warming.

Beyond the broad agreement with previous global assessments, the present biome-resolved analysis reveals several important divergences that extend current understanding of terrestrial evapotranspiration dynamics under climate change. Most global ET investigations have emphasized large-scale mean increases in evapotranspiration associated with vegetation greening and enhanced atmospheric evaporative demand (Zhang et al., 2015; Yang et al., 2023), yet relatively few studies have systematically evaluated how these responses vary across biome-specific seasonal regimes. In the present study, 86.3% of biome–month combinations exhibited positive Sen slopes, confirming the dominant global intensification signal reported in multi-dataset syntheses such as Wu et al. (2025), who estimated a global ET increase of approximately 0.65 mm yr^{-1} during 1980–2020. However, our results additionally demonstrate that the magnitude, timing, and persistence of ET_a trends differ substantially among ecosystem types. Temperate broadleaf and mixed forests exhibited the strongest annual and monthly increases, with monthly Sen slopes reaching approximately +0.292 mm $month^{-1}$ during June, whereas deserts and xeric shrublands experienced persistent summer declines reaching −0.164 mm $month^{-1}$. These contrasting responses indicate that global ET intensification is increasingly spatially heterogeneous and cannot be adequately interpreted through globally averaged trends alone. This observation supports the argument of Wu et al. (2023), who demonstrated that many existing ET products fail to fully capture evapotranspiration heterogeneity across complex and hydrologically vulnerable landscapes. By resolving ET_a dynamics at the biome level and across seasonal-to-monthly scales, the present study reveals hydroclimatic contrasts that are frequently obscured in coarse-scale global analyses.

The seasonal asymmetry detected in this study also provides new insight into the climatic sensitivity of different biome classes. Previous studies have shown that ET responses to warming vary strongly between humid and arid systems because of differing controls of energy availability and moisture limitation (Tabari & Talaee, 2014; Li et al., 2021). Our findings strongly support this framework. Forest-dominated and high-latitude biomes displayed widespread positive trends during spring and summer, while water-limited Biomes exhibited either weak increases or significant declines during warm seasons. In particular, the Boreal Forests/Taiga biome showed an unusual winter reversal characterized by dominant decreasing trends despite strong positive responses during the growing season. This pattern may reflect complex cold-season hydroclimatic feedbacks involving snowpack dynamics, frozen soils, reduced radiation availability, and shifts in winter atmospheric circulation. Similar seasonal reorganizations of ET under warming have been reported by Feng et al. (2018), who identified stronger cold-season ET increases across China despite relatively weaker summer trends. Furthermore, the persistent negative summer responses observed in Mediterranean and desert Biomes are highly consistent with studies indicating that rising vapor pressure deficit and declining soil moisture increasingly suppress evapotranspiration under prolonged warming and drought stress (Albano et al., 2022; Giardina et al., 2023). These findings collectively suggest that future ET trajectories will likely become progressively polarized between energy-limited systems, where warming enhances transpiration, and moisture-limited systems, where hydrological constraints increasingly dominate ecosystem responses.

The mechanistic basis of the observed ET_a intensification appears closely linked to the interaction between vegetation dynamics, atmospheric demand, and ecosystem water accessibility. Strong positive ET_a trends in temperate and boreal forests likely reflect the combined effects of vegetation greening, extended growing seasons, increased leaf area index, and enhanced transpiration efficiency under warming conditions (Yang et al., 2023). High-latitude Biomes are particularly sensitive to warming-induced changes because increasing temperature enhances both biological productivity and atmospheric moisture demand while simultaneously reducing snow-cover duration and frozen-soil constraints. The elevated ET_a responses detected in tundra and boreal systems therefore align with evidence that northern Biomes are experiencing accelerated hydroclimatic amplification under ongoing climate change (Ma et al., 2020). In contrast, arid and semi-arid Biomes exhibited substantially weaker or negative ET_a responses, especially during summer months when evaporative demand peaks. This behavior likely reflects the transition from

energy limitation toward severe soil-moisture limitation, where vegetation can no longer sustain transpiration despite increasing atmospheric demand. Deep-learning and flux-based studies have shown that dryland Biomes often experience abrupt reductions in ET once critical moisture thresholds are exceeded, whereas forests maintain relatively stable transpiration through deeper rooting systems and access to subsurface water storage (Giardina et al., 2023). The pronounced negative trends observed in deserts and Mediterranean systems in the present study therefore suggest that many dryland Biomes may already be approaching hydrological resilience thresholds under continued warming.

Another important mechanism underlying the observed ET_a variability is the increasing role of atmospheric evaporative demand and vapor pressure deficit (VPD). Several recent studies have demonstrated that warming-driven increases in VPD strongly amplify evapotranspiration responses in energy-limited environments while intensifying moisture stress in drylands (Albano et al., 2022; Li et al., 2021). The strong positive correlations observed here during the Northern Hemisphere growing season, particularly in June and July, likely reflect the synchronization of vegetation activity with enhanced atmospheric demand under favorable moisture conditions. Conversely, negative correlations in dry biomes during their dry seasons indicate that increasing atmospheric demand is no longer matched by sufficient water availability. This divergence is especially important because it implies that future ET responses may become increasingly nonlinear across biomes. Allan et al. (2020) emphasized that climate-driven intensification of the hydrological cycle does not occur uniformly, but is strongly modulated by regional circulation patterns, land-surface feedbacks, and anthropogenic influences such as land-use change and irrigation. The biome-dependent responses identified in the present study provide empirical support for this conceptual framework and further suggest that terrestrial ETa dynamics are undergoing a gradual hydroclimatic reorganization rather than a simple monotonic increase.

The findings of this study have important implications for global hydrology, ecosystem resilience, and climate adaptation planning. The widespread increase in ET_a across most global biomes suggests that terrestrial Biomes are experiencing increasing atmospheric water demand and accelerating water-cycle turnover under climate warming. Such intensification may substantially alter soil moisture regimes, vegetation productivity, runoff generation, and drought propagation processes, particularly in regions already characterized by hydrological vulnerability. The strong divergence observed between humid and dry biomes further indicates that future water security

risks are unlikely to be spatially uniform. While forested and high-latitude Biomes may continue to exhibit enhanced transpiration and vegetation activity, dryland systems may face increasing ecological stress as evaporative demand exceeds available moisture supply. These patterns are particularly relevant for arid and semi-arid regions where even modest increases in ET can significantly affect agricultural water requirements, groundwater depletion, and ecosystem stability (Goyal, 2004). Moreover, the pronounced seasonal redistribution of ET_a trends identified here suggests that climate change is altering not only the magnitude but also the timing of terrestrial water fluxes, with potential consequences for ecosystem phenology, wildfire susceptibility, and hydroclimatic extremes. Consequently, incorporating biome-specific and seasonally resolved ET responses into climate adaptation strategies, hydrological modeling frameworks, and water-resource management policies will become increasingly necessary under continued global warming.

Future research should further advance the biome-specific understanding of evapotranspiration dynamics by integrating process-based mechanisms, multi-source observations, and next-generation climate projections. Although the present study provides a comprehensive assessment of long-term ETa variability across global biomes, several important uncertainties remain regarding the relative contributions of vegetation change, atmospheric evaporative demand, soil moisture depletion, and anthropogenic disturbances to observed ET_a trends. Future investigations should therefore combine high-resolution ET products with flux-tower observations, groundwater information, vegetation physiological indicators, and Earth system model outputs to better disentangle the interacting controls governing hydroclimatic responses across Biomes. In particular, integrating recently developed multi-dataset fusion frameworks such as BMA-ET (Wu et al., 2025) with advanced process-based products like GLEAM4 (Miralles et al., 2024) could substantially reduce structural uncertainties and improve representation of spatial heterogeneity. Moreover, machine-learning and deep-learning approaches capable of resolving nonlinear water-stress responses across biomes (Giardina et al., 2023) offer considerable potential for identifying ecological thresholds, resilience limits, and abrupt hydroclimatic transitions under continued warming. Future studies should also evaluate ET_a dynamics under CMIP6 climate scenarios to assess how seasonal and biome-dependent responses may evolve under different warming pathways. Such efforts are essential for improving predictive understanding of terrestrial water-cycle reorganization and for developing adaptive strategies aimed at mitigating future water-security and ecosystem risks in a rapidly warming world.

Conclusion

This study delivers a biome-resolved, multi-scale assessment of global ET_a over 1980–2023 and demonstrates that recent changes are characterized by pronounced yet spatially uneven intensification across the terrestrial water cycle. ET_a trends do not follow a uniform global signal; instead, they diverge systematically across biomes and timescales as a function of ecohydrological structure, atmospheric evaporative demand, and water availability. Positive trends dominate energy-limited systems, particularly temperate and boreal forests and tundra, whereas arid and seasonally water-limited biomes frequently exhibit weak or negative responses, especially during warm-season periods.

Seasonal analyses further show that ET_a variability is governed by the intra-annual coupling between energy input and soil moisture dynamics. The strongest increases occur during the Northern Hemisphere growing season, when vegetation activity and atmospheric demand co-occur, while winter and late-season responses are often constrained by radiation limitation, snow processes, and declining soil moisture. These results point to an emerging divergence between energy-limited and water-limited evapotranspiration regimes under climate warming, with humid Biomes largely sustaining or enhancing ET_a and drylands becoming increasingly constrained by hydrological stress.

Overall, global ET_a is undergoing a biome-dependent reorganization rather than a spatially coherent intensification. This structural shift has important implications for land–atmosphere feedbacks, ecosystem productivity, and water-resource resilience. Although the observational framework limits formal causal attribution, the consistency of the detected patterns underscores the need for biome-specific and seasonally resolved representations of ET in Earth system models and provides a robust basis for future process-based and attribution-focused investigations.

Reference

Albano, C. M., Abatzoglou, J. T., McEvoy, D. J., Huntington, J. L., Morton, C. G., Dettinger, M. D., & Ott, T. J. (2022). A multidataset assessment of climatic drivers and uncertainties of recent trends in evaporative demand across the continental United States. Journal of Hydrometeorology, 23(4), 505-519.

Allan, R.P., Barlow, M., Byrne, M.P., Cherchi, A., Douville, H., Fowler, H.J., Gan, T.Y., Pendergrass, A.G., Rosenfeld, D., Swann, A.L.S., Wilcox, L.J. and Zolina, O. (2020), Advances in understanding large-scale responses of the water cycle to climate change. Ann. N.Y. Acad. Sci., 1472: 49-75. https://doi.org/10.1111/nyas.14337

Alsafadi, K., Bashir, B., Mohammed, S., Abdo, H.G., Mokhtar, A., Alsalman, A., & Cao, W. (2024). Response of Ecosystem Carbon-Water Fluxes to Extreme Drought in West Asia. Remote Sensing, 16, 1179.

Benjamini, Y., & Hochberg, Y. (1995). Controlling the false discovery rate: A practical and powerful approach to multiple testing. Journal of the Royal Statistical Society: Series B (Methodological), 57(1), 289–300. https://doi.org/10.1111/j.2517-6161.1995.tb02031.x

Berg, A., Findell, K., Lintner, B., Giannini, A., Seneviratne, S. I., van den Hurk, B., Lorenz, R., Pitman, A., & Reichstein, M. (2016). Land–atmosphere feedbacks amplify aridity increase under global warming. Nature Climate Change, 6(9), 869–874. https://doi.org/10.1038/nclimate3028

Dinerstein, E., Olson, D., Joshi, A., Vynne, C., Burgess, N. D., Wikramanayake, E., ... & Saleem, M. (2017). An ecoregion-based approach to protecting half the terrestrial realm. BioScience, 67(6), 534-545.

Feng, T., Su, T., Ji, F., Zhi, R., & Han, Z. (2018). Temporal characteristics of actual evapotranspiration over China under global warming. Journal of Geophysical Research: Atmospheres, 123, 5845–5858. https://doi.org/10.1029/2017JD028227

Flerchinger, G. N., Hanson, C. L., & Wight, J. R. (1996). Modeling evapotranspiration and surface energy budgets across a watershed. Water Resources Research, 32(8), 2539-2548.

for Statistical Computing, Vienna, Austria. https://www.R-project.org/

Gentine, P., Green, J. K., Guérin, M., Humphrey, V., Seneviratne, S. I., Zhang, Y., & Zhou, S. (2019). Coupling between the terrestrial carbon and water cycles—a review. Environmental Research Letters, 14(8), 083003.

Giardina, F., Gentine, P., Konings, A. G., Seneviratne, S. I., & Stocker, B. D. (2023). Diagnosing evapotranspiration responses to water deficit across biomes using deep learning. New Phytologist, 240(3), 968–983. https://doi.org/10.1111/nph.19197

Goyal, R. K. (2004). Sensitivity of evapotranspiration to global warming: a case study of arid zone of Rajasthan (India). Agricultural water management, 69(1), 1-11.

Guo, X., Meng, D., Chen, X., & Li, X. (2022). Validation and Comparison of Seven Land Surface Evapotranspiration Products in the Haihe River Basin, China. Remote Sensing, 14, 4308.

Hamed, K. H., & Rao, A. R. (1998). A modified Mann–Kendall trend test for autocorrelated data. Journal of Hydrology, 204(1–4), 182–196. DOI: 10.1016/S0022-1694(97)00125-X

Hayat, M., Xu, X., & Liu, R. (2025). Hydroclimatic constraints on tree transpiration-induced cooling across global biomes. Geophysical Research Letters, 52, e2024GL113551. https://doi.org/10.1029/2024GL113551

Helbig, M., Waddington, J.M., Alekseychik, P., Amiro, B.D., Aurela, M., Barr, A.G., Black, T.A., Blanken, P.D., Carey, S.K., Chen, J., Chi, J., Desai, A.R., Dunn, A.L., Euskirchen, E.S., Flanagan, L.B., Forbrich, I., Friborg, T., Grelle, A., Harder, S., Heliasz, M., Humphreys, E.R., Ikawa, H., Isabelle, P., Iwata, H., Jassal, R.S., Korkiakoski, M., Kurbatova, J., Kutzbach, L., Lindroth, A., Löfvenius, M.O., Lohila, A., Mammarella, I., Marsh, P., Maximov, T., Melton, J.R., Moore, P.A., Nadeau, D.F., Nicholls, E.M., Nilsson, M.B., Ohta, T., Peichl, M., Petrone, R.M., Petrov, R., Prokushkin, A.S., Quinton, W.L., Reed, D.E., Roulet, N.T., Runkle, B., Sonnentag, O., Strachan, I.B., Taillardat, P., Tuittila, E., Tuovinen, J., Turner, J., Ueyama, M., Varlagin, A., Wilmking, M., Wofsy, S.C., & Zyrianov, V. (2020). Increasing contribution of peatlands to boreal evapotranspiration in a warming climate. Nature Climate Change, 10, 555-560.

Hofmann, G.S., Weber, E.J., Bastazini, V.A., Rossatto, D.R., Franco, A.C., Granada, C.E., Kaminski, L.A., Ubaid, F.K., Leandro-Silva, V., Borges-Martins, M., Silva, R.C., Cardoso, M., Oliveira, L.F., Aquino, F.E., & Pereira, M.J. (2025). Climate Change in the Brazilian Cerrado: A Looming Threat to Terrestrial Biodiversity. Wiley Interdisciplinary Reviews: Climate Change, 16.

Kendall, M. G. (1975). Rank Correlation Methods (4th ed.). Charles Griffin.

Li, S., Wang, G., Sun, S., Hagan, D. F. T., Chen, T., Dolman, H., & Liu, Y. (2021). Long-term changes in evapotranspiration over China and attribution to climatic drivers during 1980–2010. Journal of Hydrology, 595, 126037.

Liu, J., You, Y., Li, J., Sitch, S., Gu, X., Nabel, J. E., ... & Kong, D. (2021). Response of global land evapotranspiration to climate change, elevated CO2, and land use change. Agricultural and Forest Meteorology, 311, 108663.

Ma, J., Zhou, L., Foltz, G. R., Qu, X., Ying, J., Tokinaga, H., ... & Gu, X. (2020). Hydrological cycle changes under global warming and their effects on multiscale climate variability. Annals of the New York Academy of Sciences, 1472(1), 21-48.

Ma, X., Zhao, C., Tao, H., Zhu, J., & Kundzewicz, Z. W. (2018). Projections of actual evapotranspiration under the 1.5 C and 2.0 C global warming scenarios in sandy areas in northern China. Science of the Total Environment, 645, 1496-1508.

Mann, H. B. (1945). Nonparametric tests against trend. Econometrica, 13(3), 245–259. https://doi.org/10.2307/1907187

Martens, Brecht, et al. "GLEAM v3: Satellite-based land evaporation and root-zone soil moisture." Geoscientific Model Development 10.5 (2017): 1903-1925. https://doi.org/10.5194/gmd-10-1903-2017

Maruyama, T., Segawa, M., & Takimoto, H. (2025). Estimation of sensible and latent heat flux and evapotranspiration in arid regions using inverse analysis. Hydrological Sciences Journal, 70(1), 162-175.

Miralles, D. G., Bonte, O., Koppa, A., Baez-Villanueva, O. M., Tronquo, E., Zhong, F., ... & Haghdoost, S. (2025). GLEAM4: global land evaporation and soil moisture dataset at 0.1 resolution from 1980 to near present. Scientific data, 12(1), 416.

Miralles, D. G., Bonte, O., Koppa, A., Villanueva, O. B., Tronquo, E., Zhong, F., ... & Haghdoost, S. (2024). GLEAM4: global land evaporation dataset at 0.1 resolution from 1980 to near present.

Miralles, D. G., Jiménez, C., Jung, M., Michel, D., Ershadi, A., McCabe, M. F., ... & Fernández-Prieto, D. (2016). The WACMOS-ET project–Part 2: Evaluation of global terrestrial evaporation data sets. Hydrology and Earth System Sciences, 20(2), 823-842.

Pan, S., Pan, N., Tian, H., Friedlingstein, P., Sitch, S., Shi, H., Arora, V. K., Haverd, V., Jain, A. K., Kato, E., Lienert, S., Lombardozzi, D., Nabel, J. E. M. S., Ottlé, C., Poulter, B., Zaehle, S., & Running, S. W. (2020). Evaluation of global terrestrial evapotranspiration using state-of-the-art approaches in remote sensing, machine learning and land surface modeling. Hydrology and Earth System Sciences, 24(3), 1485–1509. https://doi.org/10.5194/hess-24-1485-2020

Patakamuri, S. K., & O'Brien, N. (2020). modifiedmk: Modified Mann-Kendall Trend Tests.

R Core Team. (2023). R: A Language and Environment for Statistical Computing. R Foundation

R package version 1.6.0. https://CRAN.R-project.org/package=modifiedmk

Sen, P. K. (1968). Estimates of the regression coefficient based on Kendall's tau. Journal of the American Statistical Association, 63(324), 1379–1389. https://doi.org/10.1080/01621459.1968.10480934

Tabari, H., & Talaee, P. H. (2014). Sensitivity of evapotranspiration to climatic change in different climates. Global and Planetary Change, 115, 16-23.

Von Storch, H. (1995). Misuses of statistical analysis in climate research. In H. von Storch & A. Navarra (Eds.), Analysis of Climate Variability: Applications of Statistical Techniques (pp. 11–26). Springer. https://doi.org/10.1007/978-3-662-03167-4_2.

Wilks, D. S. (2016). "The stippling shows statistically significant grid points": How research results are routinely overstated and overinterpreted, and what to do about it. Bulletin of the American Meteorological Society, 97(12), 2263–2273. https://doi.org/10.1175/BAMS-D-15-00267.1

Wu, J., Feng, Y., Zheng, C., & Zeng, Z. (2023). Dense flux observations reveal the incapability of evapotranspiration products to capture the heterogeneity of evapotranspiration. Journal of Hydrology, 622, 129743.

Wu, Y., Miao, C., Wang, Y., Zhang, Q., Ji, J., & Chai, Y. (2025). Multi-spatial scale assessment and multi-dataset fusion of global terrestrial evapotranspiration datasets. Earth System Science Data Discussions, 2025, 1-27.

Xiao, J., Baldocchi, D., Ichii, K., Li, F., & Papale, D. (2026). Insights into terrestrial carbon and water cycling from the global eddy covariance network. Nature Reviews Earth & Environment, 7(1), 60-79.

Yang, Y., Roderick, M. L., Guo, H., Miralles, D. G., Zhang, L., Fatichi, S., ... & Yang, D. (2023). Evapotranspiration on a greening Earth. Nature Reviews Earth & Environment, 4(9), 626-641.

Zhang, K., Kimball, J. S., Nemani, R. R., Running, S. W., Hong, Y., Gourley, J. J., & Yu, Z. (2015). Vegetation greening and climate change promote multidecadal rises of global land evapotranspiration. Scientific reports, 5(1), 15956.

Zhu, Z., Piao, S., Myneni, R. B., Huang, M., Zeng, Z., Canadell, J. G., Ciais, P., Sitch, S., Friedlingstein, P., Arneth, A., et al. (2016). Greening of the Earth and its drivers. Nature Climate Change, 6(8), 791–795. https://doi.org/10.1038/nclimate3004

Acknowledgements

The authors gratefully acknowledge the use of the GLEAM v4 datasets, which provided critical support for the data analysis conducted in this study. We also extend our sincere thanks to the International Institute for Applied Systems Analysis (IIASA) for their institutional support, as well as to the Iran National Science Foundation (INSF) for their financial and academic support, which made this research possible.

Funding: This work is based upon research funded by Iran National Foundation (INSF) Uunder project No. 4036990

Author Contributions:

Mohammad Kamangar: Conceptualization, Methodology, Formal analysis, Investigation, Writing – original draft.
Sylvia Tramberend: Methodology, Validation, Writing – review & editing.
Masoud Minaei: Data curation, Investigation, Visualization.
Emilio Politti: Supervision, Methodology, Writing – review & editing.

Ethical Approval

This study did not require ethical approval.

Consent to Participate

This is not applicable.

Consent to Publish

This is not applicable.

Competing Interests:

The authors declare that there is no conflict of interest regarding the publication of this manuscript.

Availability Statement

The evapotranspiration data used in this study were obtained from GLEAM v4 (https://www.gleam.eu). The analysis code is available from the corresponding author upon reasonable request.